Simulating Nozzle Flow and Sprays Using An Eulerian Two-Phase Flow Model with a Realistic Equation of State

Y. Wang, R. D. Reitz*
Engine Research Center, University of Wisconsin-Madison, U.S.A.
yuewang05@gmail.com and reitz@engr.wisc.edu

Abstract

The internal flow in a fuel injector nozzle and the external spray atomization are closely related. As a result, CFD modeling of sprays must properly take into account the influence of the nozzle flow. Before its complete atomization into droplets, the fuel is in the form of continuous liquid column in the near-nozzle region. An Eulerian CFD approach assumes a continuum two-phase fluid both inside and outside of the nozzle, and hence provides a natural coupling between the two flows. Most previous studies using the Eulerian approach assume incompressibility. However, considering the fact that the sound speed is greatly reduced in the two-phase regime, this assumption limits the model's application to high-speed fuel injection cases.

The current study presents an equilibrium Eulerian approach for compressible flows. For single-component flows, the thermodynamic states and phase transition are modeled with the Stiffened Gas Equations [1, 2] implemented in the KIVA-3V code. The model is then extended to two-component flows under the assumption of ideal mixing, with one component being inert air. The methodology of the model and its validation against classical two-phase flow problems are presented.

Introduction

The processes and outcomes of fuel injection and atomization are of central importance for fuel-air mixing and combustion in diesel or gasoline-direct-injection engines. The mechanism of atomization and its controlling factors are of great interest to both scientists and engineers. During the past two decades, more and more attention has been placed on the deterministic role of the internal injector flow. Takami *et al* [3] demonstrated the effects of different nozzle inlet shapes on atomization outcomes. Sou *et al* [4] observed strong correlations between nozzle internal cavitation and external ligament formation, the latter of which is considered to be a precursor to the full atomization of a liquid jet. Phase change of fuel inside the nozzle is acknowledged as an effective way of enhancing atomization, and has been recently termed "thermodynamic breakup" [5].

An efficient CFD approach for two-phase flows is to model one phase as continuum and the other relatively dispersed phase as discrete particles. For example, inside the nozzle liquid fuel is a continuum and cavitated bubbles are particles [6]; outside the nozzle liquid fuel is broken up into particles (drops), and the mixture of air and fuel vapor is the continuum [7]. Difficulty arises when integrating nozzle flow and sprays into one simulation, and a model is required at the nozzle exit to couple the two approaches. A fully continuum-based (or "Eulerian") model for both phases avoids such difficulties and introduces no model into the coupling.

However, typical Eulerian CFD modeling requires the grid size to be sufficiently small compared to the scales of the continuum fluid. The best-resolved and the most reliable approach is Direct Numerical Simulation (DNS) with interface-tracking techniques [8, 9], aiming at capturing most scales and interfacial details. However, super-computer facilities and huge amount of CFD hours limits its application outside academia. As a compromise, the Large-Eddy simulation (LES) method only resolves motions and structures on the large scale (usually the grid size) and leaves the small (sub-grid) scales to modeling [10-13]. The sub-grid modeling for two-phase flow problems is also challenging unless the grid is sufficiently refined, but in such cases the distinction between LES and DNS is not that clear. Besides, when phase transition is considered, the rate of mass transfer between the liquid and vapor must be modeled, which involves empirical correlations and tunable parameters [14].

Eulerian modeling can be simplified by assuming homogeneous mixing in each computational cell without tracking of interfaces. In any case, details of interface phenomena are not of interest in local regions with large Weber numbers until the flow reaches far downstream of nozzle exit and fully atomizes. In this sense, the fuel-air two-phase mixture is very similar on large scales to a gas jet with density variation. This mixture-based or "one-fluid" methodology does not need a phase or "tracker" continuity equation, and the grid size required can be flexible, depending on the level of turbulence to be resolved [15-17].

The challenge to the one-fluid approach is to find a realistic Equation of State (EOS) to describe the thermodynamic properties of the mixture. Since interfacial phenomena are not modeled, this EOS should also predict

* Corresponding author: reitz@engr.wisc.edu

phase change on the macroscopic (i.e., grid size) level. The EOS should predict thermodynamic equilibrium because this is how the thermodynamic states are defined. However, the most widely-used barotropic EOS [18, 16, 17], also called "homogeneous equilibrium model", does not predict the equilibrium states. It does not consider the 2nd law of thermodynamics, which provides the appropriate conditions of equilibrium. In the two-phase regime, the isotherm of this EOS has non-negative slope for pressure as a function of density, and hence does not provide a valid value for the vapor pressure at the local temperature.

It was argued in [19] that one might skip the complication of EOS by modeling phase change under the framework of non-equilibrium thermodynamics. While the non-equilibrium approach might admit application to a broader range of problems, it is expected that proper equilibrium solutions should be reached under certain circumstances. In other words, the equilibrium approach should be incorporated as a particular solution into a more general non-equilibrium solver. This idea has been detailed in [1, 2], where a rigorous derivation of equilibrium conditions based on thermodynamic principles was coupled with a CFD solver.

In the present study, equilibrium models for the single-component flows of Ref. [1] are implemented into the KIVA-3V Release 2 code [20]. The code is then extended to two-component flows, with one component being air that does not change phase. Validations using classical real flow problems are presented and discussed.

Phase Equilibrium Model for Single-Component Flows

The phase equilibrium model of Ref. [1] is briefly reviewed. The focus is on its practical implementation into a CFD solver and validations. Consider a certain computational cell containing a mixture of liquid and vapour. The mixture specific volume v and internal energy ε are obtained from the conservation laws and regarded as inputs to the model. The entropy of the mixture can be expressed by adding the entropies of two phases:

$$s = ys^v\left(v^v, \varepsilon^v\right) + \left(1-y\right)s^l\left(v^l, \varepsilon^l\right) \tag{1}$$

where y is the mass fraction of vapour. Superscripts v and l indicate properties of the individual phases. The specific volume and internal energy of each phase can be related to the corresponding mixture properties with:

$$v^v = \frac{\alpha}{y}v, \quad v^l = \frac{1-\alpha}{1-y}v; \qquad \varepsilon^v = \frac{z}{y}\varepsilon, \quad \varepsilon^l = \frac{1-z}{1-y}\varepsilon \tag{2}$$

where α and z are the volume and energy fractions of the vapor phase, respectively. It has been assumed that the vapor and liquid phases are immiscible, so that their volumes add up to the volume of the computational cell. From thermodynamics, the two-phase mixture's entropy is maximized when phase equilibrium is achieved, i.e.:

$$s\left(v, \varepsilon, \left(y, \alpha, z\right)_{eq}\right) = \max s\left(v, \varepsilon, \left(y, \alpha, z\right)\right) \tag{3}$$

This gives the three conditions of equilibrium as:

$$\frac{p^v}{T^v} - \frac{p^l}{T^l} = 0; \quad \frac{1}{T^v} - \frac{1}{T^l} = 0; \quad \frac{g^v}{T^v} - \frac{g^l}{T^l} = 0 \tag{4}$$

Namely, the pressures, temperatures and Gibbs functions ($g = pv + \varepsilon - Ts$) of the two phases must be equal. The pressure equilibrium condition suggests that the same pressure of a computational cell can be applied for both the liquid and vapour phase, and hence the surface tension effect can be neglected. The temperature equilibrium condition implies that heat transfer between two phases is infinitely fast compared to the flow time scales. Together with the phase equilibrium condition of Gibbs function, the conditions make sure that at every time step the fluid is at the correct equilibrium composition, since the mixture specific volume (or density) and internal energy are determined by the mass and energy conservation laws of fluid mechanics.

In this study, the above approach was implemented into the KIVA-3V Release 2 code [20]. The Stiffened Gas Equations of States [21] are used to describe the physical properties of the liquid and vapour. For each phase, the Stiffened Gas Equations consist of a pressure law and a caloric law:

$$\text{for vapor: } \begin{cases} p + \pi^v = C^v\left(\gamma^v - 1\right)\dfrac{T}{v^v} \\ \varepsilon^v = C^vT + Q^v + \pi^v v^v \end{cases} \qquad \text{for liquid: } \begin{cases} p + \pi^l = C^l\left(\gamma^l - 1\right)\dfrac{T}{v^l} \\ \varepsilon^l = C^lT + Q^l + \pi^l v^l \end{cases} \tag{5}$$

in which C, Q and π are parameters. The phase equilibrium solver requires inputs of the mixture's specific volume v and internal energy ε. In light of (2), they can be related to the phase properties by:

$$v = yv^v + \left(1-y\right)v^l; \quad \varepsilon = y\varepsilon^v + \left(1-y\right)\varepsilon^l \tag{6}$$

Given the vapor mass fraction y, simultaneous solutions of Eqns. (5) and (6) result in a quadratic equation for either v^l or v^v. It is found in practice that one of the two roots is always unphysical and the other physical root should be taken. The full solution of Eqns. (5) and (6) is then examined using Gibbs function condition in Eq. (4). A guessed value of y is updated with a Newton iteration until this condition is met. If a single-phase instead of two-phase state exists for the given inputs v and ε, the vapor fraction y tends to converge to a negative value or a value larger than 1.0. In this case, a liquid or vapor single-phase solution should be taken, respectively.

KIVA [20] solves the conservation laws at each time step in three consecutive phases: In Phase A the cell is static, and the source terms for the spray particles and chemistry are solved. In this study, Phase A is irrelevant because non-reactive Eulerian flow is of interest. In Phase B the cell is moved with the local fluid, and all the physics (pressure effect, diffusion, etc.), except for convection solved. Finally, in Phase C the cell boundaries are mapped back to the position where they should be, as determined by specified mesh motion.

The above-mentioned equilibrium solver was implemented at the end of Phase C, when the flow convection calculation is completed and pressure field is to be updated. In Phase B, the phase composition is assumed to be "frozen" while the energy equation and pressure correction are solved in the SIMPLE loop. This is generally a good assumption within a reasonably small time step, unless the fluid in its pure liquid state expands and reaches the bubble point. When this happens, assuming an unchanged phase composition results in negative pressures, due to the large isentropic sound speed of the liquid. In this case, the phase equilibrium solver is called to compute a two-phase solution and its corresponding (reduced) sound speed, and a negative pressure is prevented.

To validate the code, the shock tube problem of Ref. [1] is investigated. The problem considers a simple model fluid, of which the EOSs for both phases are reduced to perfect gas relations. As seen in Table 1, the only difference between the two phases is the specific heat ratio γ: the liquid phase has a smaller γ and is denser. Consider the 1-D Riemann problem with an initial discontinuity separating the left (L) and right regions (R) with:

Right region (0.5 to 1.0 m): $p_R = 0.1$ Pa, $v_R = 1.3$ m^3/kg, $u_R = 0$ (vapor)

Left region (0 to 0.5m): $p_L = 1.445$ Pa, $v_L = 0.92$ m^3/kg, $u_L = 0.13$ m/s (2-phase mixture)

Parameters	C	γ	π	Q	v_0	T_0	s_0
Unit	[J/Kg-K]	[-]	[Pa]	[J/Kg]	[m^3/kg]	[K]	[J/Kg-K]
Perfect Gas Model (Vapor)	1.0	1.600	0.0	0.0	0.0	1.0	0.0
Perfect Gas Model (Liquid)	1.0	1.500	0.0	0.0	0.0	1.0	0.0
Water (Vapor)	1615.0	1.300	0.0	1.892e6	1.0e8	100.0	13880.0
Water (Liquid)	1400.0	3.000	9.0e8	-1.048e6	1.0e-8	100.0	-32750.0
Air	726.6	1.395	0.0	0.0	N/A	N/A	N/A

Table 1 Parameters of stiffened gas equations for different fluids

It was shown in Ref. [1] that the analytical solution consists of a shock propagating to the right. The flow region behind this shock is filled with saturated vapor. This region is ahead of another shock and followed by the intermediate 2-phase region. The intermediate region has higher density and pressure than the left region, leading to another shock propagating to the left. Figure 1 shows CFD predictions using the modified KIVA code compared to the analytical solutions at 0.5 s. The three shocks and one contact surface are all captured, and the predictions of their positions and strength are precise. Behind the first right-running shock where the fluid is supposed to be saturated vapor, the simulation predicts the fluid to be two-phase, with 92% vapor and 8% liquid. This leads to a slight over-prediction of density and pressure. However, speaking overall, the agreement is good and this validates the algorithm implementation.

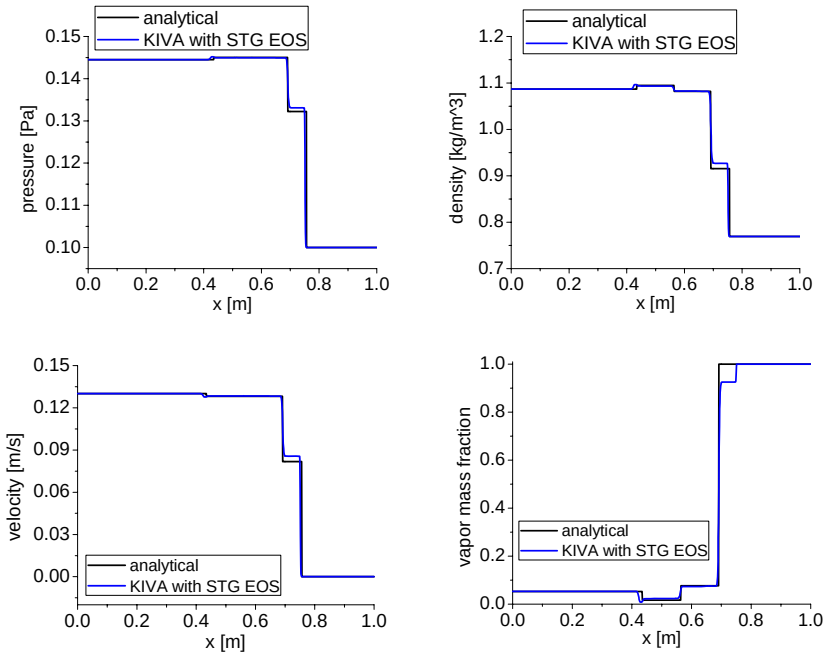

Figure 1 CFD results compared to analytical solutions for the shock tube problem

Next, a real flow problem of water flows is studied to further examine the model. The Stiffened Gas Equation parameters for water are also summarized in Table 1. These parameters provide accurate matching to property data for the liquid, two-phase, and vapour regimes, as shown in Figure 2. The water-steam converging-diverging nozzle experiment of Neusen [22] was modelled by specifying pressure and vapour mass fraction (or quality) at the nozzle inlet ("0"). The two-phase mixture enters the convergent section and is accelerated to the speed of sound at the throat ("*"), and then expands to supersonic speeds in the divergent section. During the expansion process, significant pressure drop occurs and this turns the water into steam. When the local pressure drops below the vapour pressure, the flow is 100% vapour. Figure 3 plots the normalized pressure profile against normalized cross-sectional area. The simulation catches the trend of pressure drop very well, especially for the value of pressure at the throat. Under-prediction occurs in the divergent section, notably for the small quality case. This indicates an over-prediction of the evaporation rate likely due to the phase equilibrium assumption.

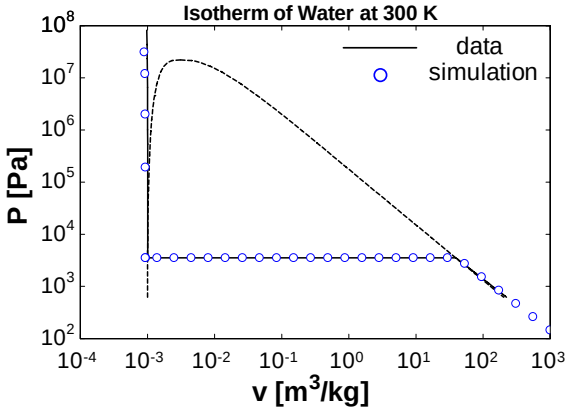

Figure 2 Isotherm of water at 300 K

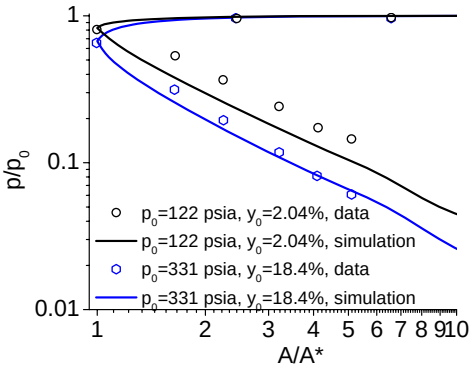

Figure 3 Pressure profile of water-steam flow in a converging-diverging nozzle

Phase Equilibrium Model for Two-Component Flows

When extending the model to two-component flows, the primary interest is to study the mixture of an inert gas (denoted as fluid "1") and the other fluid with phase change ("2"). This is the case of injecting fuel into air, with the fuel modelled by a single-component substance or a surrogate mixture of components. The liquid phase is made up of pure-component fuel; while the gas phase is a mixture of fuel vapour and air. Assuming an ideal gaseous mixture, its molar specific entropy can be expressed by the summability relation [23]:

$$s^g = \sum_{i=1,2} x_i^g \left.\frac{\partial S^g}{\partial n_i}\right|_{\substack{T^g, p^g, \\ n_j, j\neq i}} \tag{7}$$

where x_i^g is the mole fraction of component i in the gaseous mixture. According to Gibbs' rule [23], the partial molar entropy of a constituent species is equal to the molar entropy of the species as a pure ideal gas at the mixture temperature T^g, but at a pressure equal to its partial pressure in the mixture. Thus, Equation (7) is written as:

$$s^g = \sum_i x_i^g s_i^g \left(T^g, p_i^g\right) \tag{8}$$

in which p_i^g are partial pressures and they add up to the total pressure of the gaseous mixture:

$$p_1^g + p_2^g = p^g \tag{9}$$

The ideal mixture assumption suggests that the molecules of each species act independently and occupy the total volume of the vapor mixture:

$$p_i^g = \frac{n_i \bar{R} T^g}{V^g} = \frac{\bar{R} T^g}{v_i^g} \tag{10}$$

In light of this, Equation (8) is re-written by replacing the independent variables by specific volume and internal energy, under the same temperature and partial pressures. Superscripts "g" are dropped for air without confusion:

$$s^g = x_1 s_1\left(v_1, \varepsilon_1\right) + x_2^g s_2^g \left(v_2^g, \varepsilon_2^g\right) \tag{11}$$

Taking the liquid phase into account, its entropy is added to Eq. (12) because the two phases are immiscible:

$$s = x_1 s_1\left(v_1, \varepsilon_1\right) + x_2^g s_2^g \left(v_2^g, \varepsilon_2^g\right) + \left(1 - x_1 - x_2^g\right) s_2^l \left(v_2^l, \varepsilon_2^l\right) \tag{12}$$

In order to relate the species properties to the two-phase mixture's properties, the liquid volume fraction α^l, and the vapor energy fraction z_1 and z_2^g are introduced:

$$s = x_1 s_1\left(\frac{1-\alpha^l}{x_1}v, \frac{z_1}{x_1}\varepsilon\right) + x_2^g s_2^g\left(\frac{1-\alpha^l}{x_2^g}v, \frac{z_2^g}{x_2^g}\varepsilon\right) + \left(1-x_1-x_2^g\right)s_2^l\left(\frac{\alpha^l}{1-x_1-x_2^g}v, \frac{1-z_1-z_2^g}{1-x_1-x_2^g}\varepsilon\right) \tag{13}$$

Phase equilibrium is modeled with the same entropy maximization criterion as described in Equation (3). But in this case, besides the mixture v and ε, the mole fraction of air x_1 is also a specified variable since it is fixed by mass conservation of the fluid solver. Thus, criterion (3) changes to:

$$s\left(x_1, v, \varepsilon, \left(x_2^g, \alpha^l, z_1, z_2^g\right)_{eq}\right) = \max s\left(x_1, v, \varepsilon, \left(x_2^g, \alpha^l, z_1, z_2^g\right)\right) \tag{14}$$

Maximum entropy yields the following four equilibrium conditions:

$$\left.\frac{\partial s}{\partial \alpha^l}\right|_{x_2^g, z_1, z_2^g} = 0 \;\Rightarrow\; \frac{p_1}{T_1} + \frac{p_2^g}{T_2^g} - \frac{p_2^l}{T_2^l} = 0 \qquad \left.\frac{\partial s}{\partial z_1}\right|_{x_2^g, \alpha^l, z_2^g} = 0 \;\Rightarrow\; \frac{1}{T_1} - \frac{1}{T_2^l} = 0$$
$$\left.\frac{\partial s}{\partial z_2^g}\right|_{x_2^g, \alpha^l, z_1} = 0 \;\Rightarrow\; \frac{1}{T_2^g} - \frac{1}{T_2^l} = 0 \qquad \left.\frac{\partial s}{\partial x_2^g}\right|_{\alpha^l, z_1, z_2^g} = 0 \;\Rightarrow\; g_2^g = g_2^l \tag{15}$$

The first three conditions can be reformulated to a pressure equilibrium and a thermal equilibrium condition:

$$p_1 + p_2^g = p_2^l := p \qquad T_1 = T_2^g = T_2^l := T$$

Notice that temperature equilibrium has been assumed when making the analysis of mixture entropy in Eqs. (8) and (12). In the fourth condition of Eq. (16), the Gibbs function for the vapor phase is evaluated at the partial pressure instead of the total pressure:

$$g_2^g = \varepsilon_2^g + p_2^g v_2^g - T s_2^g \qquad g_2^l = \varepsilon_2^l + p_2^l v_2^l - T s_2^l$$

It is well known that phase equilibrium of a species requires that the chemical potentials, or partial molar Gibbs energies of both phases must be equal. In this analysis, since the liquid phase is made of a pure component, its partial molar Gibbs energy is equal to its molar Gibbs function. The vapor phase is modeled by an ideal gas mixture. With Gibbs' rule, the partial molar Gibbs energy is equal to the molar Gibbs function evaluated at the partial pressure. Therefore, the fourth condition of Eq. (15) implies that the vapor and liquid chemical potentials of fluid "2" must be equal. The classical condition of thermodynamic phase equilibrium is recovered.

The application of the phase equilibrium condition Eq. (15) is very similar to that introduced in the last section. Equation (5) is supplemented by a Stiffened Gas Equation of fluid "1" (air). Taking into account the partial pressure relations Eqns. (10)(11), the Equations of States are written as:

$$\text{pressure laws: } \begin{cases} p + \pi_2^g + \pi_1 = T\left(\dfrac{C_2^g\left(\gamma_2^g - 1\right)}{v_2^g} + \dfrac{C_1\left(\gamma_1 - 1\right)}{v_1}\right) \\ p + \pi_2^l = C_2^l\left(\gamma_2^l - 1\right)\dfrac{T}{v_2^l} \end{cases} \quad \text{caloric laws: } \begin{cases} \varepsilon_1 = C_1 T + Q_1 + \pi_1 v_1 \\ \varepsilon_2^g = C_2^g T + Q_2^g + \pi_2^g v_2^g \\ \varepsilon_2^l = C_2^l T + Q_2^l + \pi_2^l v_2^l \end{cases} \tag{16}$$

Conservation laws give the mixture specific volume v and internal energy ε, as well as air mole fraction x_1:

$$\begin{aligned} v &= x_1 v_1 + \left(1 - x_1 - x_2^g\right)v_2^l \\ x_1 v_1 &= x_2^g v_2^g \\ \varepsilon &= x_1\varepsilon_1 + x_2^g\varepsilon_2^g + \left(1 - x_1 - x_2^g\right)\varepsilon_2^l \end{aligned} \tag{17}$$

Assuming the vapor mole fraction x_2^g, simultaneous solutions of Eqs. (16) and (17) are obtained to calculate the Gibbs functions in the fourth condition of Eq. (15) and checked if it is satisfied. If not, x_2^g is updated with a Newton iteration until it converges.

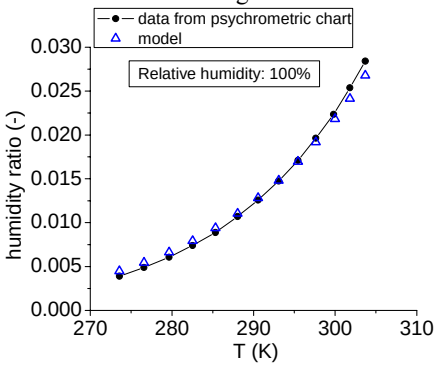

Figure 4 Model .vs. moist air data with constant π^l

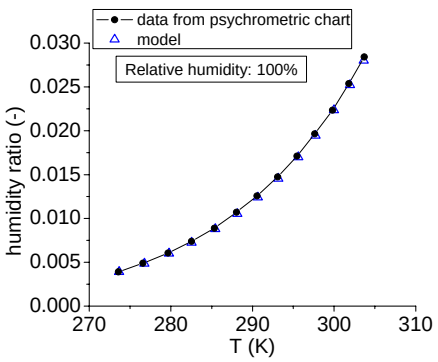

Figure 5 Model .vs. moist air data with temperature-dependent π^l

As a validation, measured data of saturated moist air was taken from a psychometric chart [24] and compared to the model predictions. The EOS parameters of water and air are those in Table 1. Figure 4 shows humidity ratio, defined as the ratio of water vapor mass to the mass of dry air, against mixture temperature. The slight difference is due to the use of a fixed value for π^l of water. It is found that, in order for the model to match vapor pressure data over a wide temperature range of 273 K to 640 K, π^l has to be varied from 8.75e8 Pa to 1.09e9 Pa. Figure 5 shows an improved prediction with a temperature-dependent π^l. However, in the following simulations temperature does not vary a lot and thus a constant π^l is used. The way to implement this equilibrium solver into KIVA is very similar to that described in the previous section.

The two-phase solver was studied with a water-air converging-diverging nozzle flow problem from Muir and Eichhorn's experiment [25]. In this experiment, air is introduced into water and mixed into a two-component, two-phase mixture, which enters the nozzle and is accelerated to the speed of sound at the throat. The flow conditions are adjusted to allow different mass flow ratios, defined as the air mass flow rate divided by the total mass flow rate, while keeping the pressure unchanged at the throat. The twelve test conditions of Ref. [25] were set up for the simulations by specifying the same mass flow ratios. Since it is assumed that the two phases have the same velocity, the mass fractions of water and air can be computed. The reported reservoir pressures P_0 are also used as inputs. Room temperature (300K) is assumed for all cases. In Table 2, the predicted air void fraction at throat is compared with data to ensure correct case setup. The results show that the relative error is at its largest 8% and is sufficiently accurate, considering the data is estimated instead of directly measured.

Test Condition	Mass flow fraction Y^*10^3	Reservoir Pressure P_0 (Psia)	Air Void Fraction at Throat α* (Data)	Air Void Fraction at Throat α* (Simulation)	Vapor Void Fraction at Throat (Simulation)
1	0.130	91.9	0.10	0.108	0.0040
2	0.183	80.0	0.13	0.138	0.0048
3	0.295	55.6	0.20	0.213	0.0078
4	0.361	50.7	0.24	0.245	0.0087
5	0.471	43.6	0.29	0.300	0.0109
5A	0.577	39.7	0.33	0.350	0.0131
6	0.734	35.3	0.40	0.406	0.0152
6A	0.922	32.0	0.45	0.460	0.0170
7	1.54	25.3	0.60	0.619	0.0275
8	2.42	21.8	0.77	0.722	0.0344
9	3.93	20.2	0.81	0.788	0.0345
10	5.46	20.1	0.86	0.834	0.0389

Table 2 Summary of Test Conditions in the Water-Air Converging-Diverging Nozzle Problem

Figure 6 shows the throat pressure, normalized by the mixing section (reservoir) pressure, plotted against mass flow fraction. The agreement is good for the cases of small mass flow fractions (Conditions 1 to 5A). At larger fractions the model under-predicts compared to the data. Also compared is Brennen's homogenous two-phase flow theory [26], which relates pressure ratio to air void fraction using:

$$\frac{\alpha^*}{1-\alpha^*} = \left[\frac{\alpha_0}{1-\alpha_0} + \frac{1}{2} \frac{p_0}{\rho^l \left(c^l\right)^2} \right] \frac{p_0}{p^*} - \frac{1}{2} \frac{p_0}{\rho^l \left(c^l\right)^2} \frac{p^*}{p_0} \tag{17}$$

The isothermal condition in Brennen's analysis is confirmed in the current simulation, since the temperature variation throughout the nozzle is found to be less than 0.3% in all cases. Substituting the air void fraction at the throat (Column 5 of Table 2) into Equation (17), the pressure ratio is found to be very close to the model prediction. Considering the evaporation of water observed in the simulation, the agreement is even better if the vapor void fraction (Column 6 of Table 2) is added to that of the air. This evaporation is due to the pressure drop associated with flow expansion. As seen in Figure 7, although the saturated vapor pressure of water (P_{sat}) is significantly smaller than the throat pressure, the present phase equilibrium model predicts only a slight amount of vapor. Its mole fraction in the gaseous mixture is very close to the ratio of P_{sat} over P^*. This agrees with the common assumption when analyzing moist air problems that P_{sat} be equal to the partial pressure of the vapor [24].

Figure 8 shows mixture velocity against void fraction of air at the throat. The data was processed by taking an average of the liquid and air flow rates. The simulation results slightly over-predict but the overall agreement is good. Figure 9 shows the measured bubble velocity compared with simulation's mixture velocity near throat. The bubbles are seen traveling at 20% larger speed, and this agrees with the observation of Ref. [25]. On the other hand, Tangren *et al.* [27] show that the mixture velocity is given by the following expression which agrees well with the simulation results.

$$u = \sqrt{2p_0/\rho_l} \left[1 - p/p_0 - \frac{\alpha_0}{1-\alpha_0} \ln\left(p/p_0\right) \right]^{1/2}$$

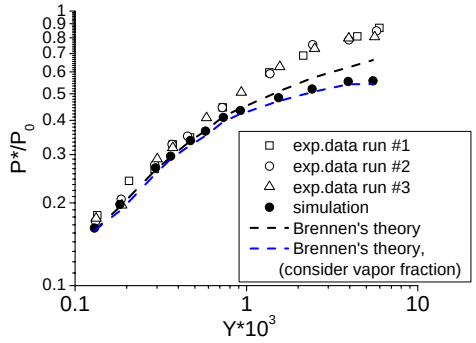

Figure 6 Throat pressure .vs. air mass flow fraction

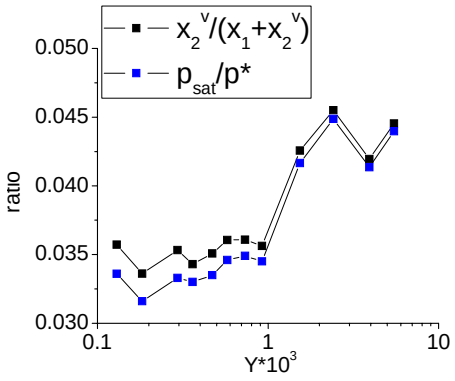

Figure 7 Vapour mole fraction and pressure

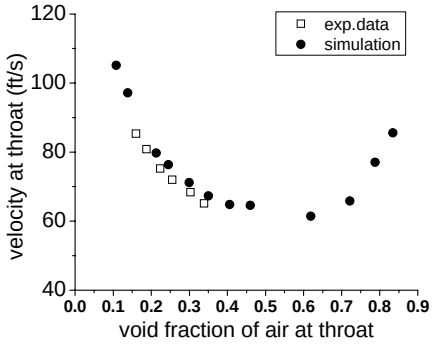

Figure 8 Mixture velocity .vs. air void fraction

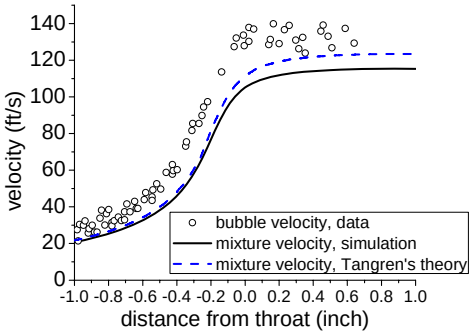

Figure 9 Near-throat velocity profile

Next, the water jet experiment of Sou et al. [28] was simulated. The experiment studied an axi-symmetric round jet injector with a sharp corner at the inlet. The diameter of the nozzle was 2mm and the length-to-diameter ratio was 4. The ratio of injection chamber cross-sectional area over nozzle cross-sectional area was 64. Water at room temperature was used as the working fluid. The injection pressure (P_{inj}) was varied while keeping the back pressure (P_b) at the atmospheric level. A cavitation number σ was defined pressure as:

$$\sigma = \frac{P_{inj} - P_v}{P_{inj} - P_b}$$

in which P_v is the vapour pressure. Cavitation was observed near the nozzle walls, and the length of the cavitated region (L_{cav}) was used as an indicator to define the flow regime. Figure 11 shows the comparison of the predicted region is compared with Sou's experiment, as a function of the cavitation number σ in Fig. 10. The variation of σ from 1.2 to 2.5 corresponds to variation of P_{inj} from 5.95 to 1.66 bar. The predicted trend agrees very well with the data, but the predicted cavitation generally occurs at a higher injection pressure. For example, super-cavitation $L_{cav} \approx L$ shown in Fig. 11 was observed at P_{inj}=3.36 bar, but was not predicted until 5.95 bar. This

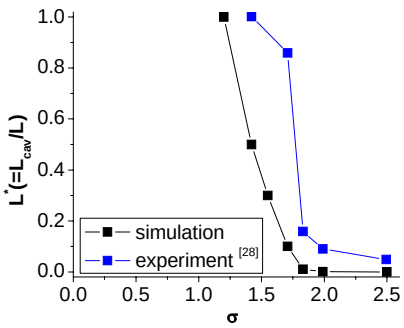

Figure 10 Cavitation length .vs. cavitation number

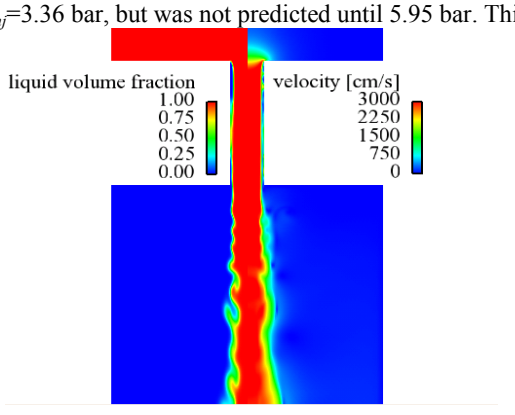

Figure 11 Predicted super-cavitation (σ=1.2)

could be due to insufficient mesh resolution. An axi-symmetric 2D mesh with only 15 cells across the nozzle was used for this demonstration of the present model's capabilities.

Summary and Conclusions

A phase equilibrium model based on the 2nd law of thermodynamics was implemented into the compressible flow solver KIVA-3V. The model considers single-component and two-component flows, with each phase of the components modelled by a Stiffened Gas Equation of State. Pressure, temperature and velocity equilibrium is assumed in each computational cell containing fluid mixture. The code was validated with an analytical shock tube problem, a water-steam and a water-air converging-diverging nozzle problem, and a cavitating water jet problem. The agreement with experimental data was generally good. The differences between prediction and data are attributed to the assumptions of equilibrium and/or mesh resolution.

The proposed approach is intended to provide the basis for future development of non-equilibrium models. More validations against experiments need to be performed to fully identify the situations where the equilibrium assumption is accurate. In particular, its application to internal combustion engine nozzle flow and sprays is of primary interest.

Acknowledgements

The authors would like to thank General Motors Company for providing the financial support and Dr. Di Diwakar for his continuous encouragement. Dr. Won-Geun Lee, Dr. Chang-Wook Lee and Mr. Lu Qiu provided much help to this research and their collegiality at the University of Wisconsin-Madison is greatly appreciated.

References

[1] Barberon, T., Helluy, P., *Computers and Fluids* 34-7: 832-858 (2005).
[2] Saurel, R., Petitpas, F., Abgrall R., *Journal of Fluid Mechanics*, 607: 313-350 (2008).
[3] Tamaki, N., Shimizu, M., Nishida, K., Hiroyasu, H., *Atomization and Sprays* 8: 179-197 (1998).
[4] Sou, A., Maulana, M. I., Hosokawa, S., Tomiyama, A., *Journal of Fluid Science and Technology* 3-5: 633-644 (2008).
[5] Negro, S., Brusiani, F., Bianchi, G. M., *SAE Technical Paper* 2011-24-0003.
[6] Giannadakis, E., Gavaises, M., Acroumanis, C., *Journal of Fluid Mechanics* 616: 153-193 (2008).
[7] Reitz, R. D., Diwakar, R., *SAE Transactions* 95-3: 218-227 (1986).
[8] Herrmann, M., *Atomization and Sprays* 21-4: 283-301 (2011).
[9] Czajkowski, M. F., Desjardins, O., *ILASS-Americas, 23rd Annual Conference on Liquid Atomization and Spray Systems*, Ventura, CA, 2011.
[10] Villiers, E., Gosman, A. D., *SAE Technical Paper* 2004-01-0100.
[11] Bianchi, G. M., Minelli, F., Scardovelli, R., Zaleski, S., *SAE Technical Paper* 2007-01-0244.
[12] Ishimoto, J., Sato, F., Sato, G., *Journal of Engineering for Gas Turbines and Power* 132: 082801 (2010).
[13] Befrui, B., Corbinelli, G., D'Onofrio, M., Varble, D., *SAE Technical Paper* 2011-01-1211.
[14] Kalata, W., Brown, K. J., Schick, R. J., *ILASS Americas, 23rd Annual Conference on Liquid Atomization and Spray Systems*, Ventura, CA, 2011.
[15] Vallet, A., Burluka, A. A., Borghi, R., *Atomization and Sprays* 11: 619-642 (2001).
[16] Lagumbay, R. S., Vasilyev, O. V., Haselbacher, A., Wang, J., *ASME 2005 International Mechanical Engineering Congress and Exposition*, Orlando, FL, 2005.
[17] Moreau, J. B., Simonin, O., Habchi, C., *ILASS-Europe*, *19th Annual Meeting of the Institute for Liquid Atomization and Spray Systems*, Nottingham, United Kingdom, 2004.
[18] Schmidt, D. P., Rutland, C. J., Corradini, M. L., *SAE Technical Paper* 971597.
[19] Schmidt, D. P., Gopalakrishnan, S., Jasak, H., International Journal of Multiphase Flow 36: 284-292 (2010).
[20] Amsden, A. A., *Los Alamos National Laboratory Report LA-13313-MS*, 1997.
[21] Harlow, F. H., Amsden, A. A., *Los Alamos National Laboratory Report LA-4700*, 1971.
[22] Neusen K. F., *B. S. Thesis*, University of California, Lawrence Radiation Laboratory, Livermore, CA; UCRL-6152, 1962.
[23] Smith, J. M., Van Ness, H. C., Abbott, M. M., *Introduction to Chemical Engineering Thermodynamics*, 6th Ed., McGraw Hill, Chap. 11, 2001.
[24] Moran, M. J., and Shapiro, H. N., *Fundamentals of Engineering Thermodyanmics*, 5th Ed., John Viley & Sons, Inc., Chap. 12, 2004.
[25] Muir, J. F., Eichhorn, R., *Proceedings of the 1963 Heat Transfer and Fluid Mechanics Institute*, Stanford University Press, pp. 183–204, 1963.
[26] Brennen, C. E., *Cavitation and Bubble Dynamics*, Oxford University Press, Chap. 6, 1995.
[27] Tangren, R. F., Dodge, C. H., Seifert, H. S., *Journal of Applied Physics* 20-7: 637 (1949).
[28] Sou, A., Maulana, M. I., K. Asozaki, Hosokawa, S., Tomiyama, A., *Journal of Fluid Science and Technology,* 3-5: 622-632 (2008).